

Binuclear Arylnickel Complexes with Bridging Bis(arylimino)-1,4-pyrazine Ligands

Axel Klein,^{*[a]} Christian Biewer,^[a] Claudia Hamacher,^[a] Natascha Hurkes,^[a] Jessica Perez Outeiral,^[a] Erik Mora Paniagua,^[a] Ann-Kathrin Schmieder,^[a] Andreas O. Schüren,^[a] Prabhakara Rao Burma,^[b] James T. Ciszewski,^[b] and David A. Vovic^[b]

Keywords: Nickel / Organometallics / Electrochemistry / Spectroelectrochemistry / EPR spectroscopy

Binuclear organometallic nickel complexes of the type $[(\mu\text{-N}^{\wedge}\text{N})\{\text{Ni}(\text{Mes})\text{Br}\}_2]$ [$\text{N}^{\wedge}\text{N}$ = α -diimine chelate ligand of the type 2,5-bis[1-(aryl)iminoethyl]pyrazine; Mes = mesityl = 2,4,6-trimethylphenyl] have been prepared and characterised electrochemically and spectroscopically in detail. A combination of NMR spectroscopy and quantum chemical calculations allowed the assignment of stereoisomers and their relative stability. The long-wavelength absorptions (600–1000 nm) assignable to charge-transfer transitions reveal a marked elec-

tronic coupling of the two metal centres over the ligand bridge via their low-lying π^* orbitals. The reversible reductive electrochemistry yields stable radical anionic complexes with mainly ligand-centred spin density as shown by electron paramagnetic resonance (EPR) spectroscopy and UV/Vis spectroelectrochemistry of the free ligands and their nickel complexes in combination with DFT calculations. Preliminary investigations of the complexes as catalysts in Negishi cross-coupling reactions gave promising results.

Introduction

Organometallic nickel complexes with α -diimine ligands such as 2,2'-bipyridine (bpy), 1,10-phenanthroline (phen) or diazabutadienes (R-DAB) have gained enormous interest in the last decade. This is mainly because of a number of important catalytic processes like olefin oligo- or polymerisation, olefin/CO co-polymerisation,^[1,2] and various (electro)catalytic C–C coupling reactions.^[3–11] Paralleling their use in catalysis, fundamental studies on structures and electronic properties of organonickel complexes with α -diimines have been carried out.^[9–18] We have contributed to this with the investigation of a number of organonickel complexes $[(\text{N}^{\wedge}\text{N})\text{Ni}(\text{Mes})\text{X}]$ ($\text{N}^{\wedge}\text{N}$ = α -diimine ligands, Mes = mesityl = 2,4,6-trimethylphenyl, X = halides) with various diimine ligands. Their structures and reactivity towards ligand exchange reactions have been studied using X-ray diffraction and absorption spectroscopy,^[14–16] their photophysics and photochemistry were explored by a combination of multiple spectroscopy and quantum chemical calculations,^[14,16,17] and finally, their redox chemistry was investigated,^[17,18] with respect to the application of such systems in electrocatalytic C–C coupling reactions.^[6]

From these studies we have a clear picture of the crucial role of the diimine ligand in these complexes. The lowest unoccupied MOs are mainly ligand(π^*)-centred, with the consequences, that both the intense colours (long-wavelength absorption bands) and the relatively low first and second reduction potentials are strongly dependent on the nature of the diimine ligand.

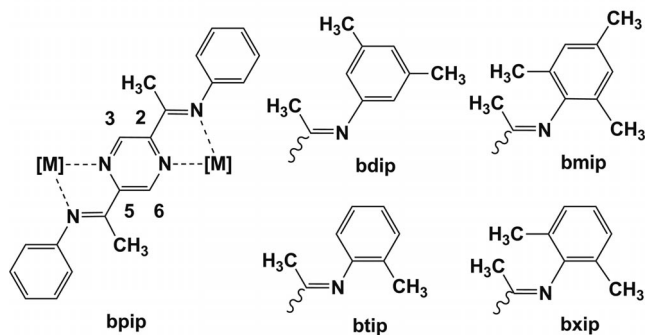
This promoted the idea of studying analogous binuclear complexes $[(\mu\text{-N}^{\wedge}\text{N})\{\text{Ni}(\text{Mes})\text{Br}\}_2]$ with bridging diimine ligands ($\text{N}^{\wedge}\text{N}$) (see Scheme 1), since we expected that the use of bridging ligands, which were able to electronically couple the two metal centres, might greatly enhance these interesting properties.^[19–21] In view of catalytical applications of such complexes binuclear derivatives are supposed to additionally offer higher thermal stability, as has been concluded in recent work.^[2]

Since the geometrical orientation of the two metal atoms might be important, we used two different types of bridging ligands. Recently we used the established ligand 2,2'-bipyridine (bpym) that allows one to direct the two metal atoms face to face, with distances of 5.5–6 Å.^[16,20] In contrast to the bpym ligand, the five ligands bpip, bdip, btip, bxip and bmp bridge the two metal atoms by a central 1,4-pyrazine unit, resulting in much larger metal–metal distances. In both cases the metal–metal interaction is not direct but supported by the bridging ligand and also herein bpym differs from the so-called *S-frame* ligands bpip–bmp,^[21] where the bridging ligand holds the two metal atoms in the two clamps of an *S*. Importantly, from the viewpoint of metal–

[a] Department für Chemie, Institut für Anorganische Chemie, Universität zu Köln, Greinstraße 6, 50939 Köln, Germany
E-mail: axel.klein@uni-koeln.de

[b] Department of Chemistry, University of Hawaii, 2545 McCarthy Mall, Honolulu, HI 96822, USA
Supporting information for this article is available on the WWW under <http://dx.doi.org/10.1002/ejic.201101436>.

[M] = transition metal complex (fragment)



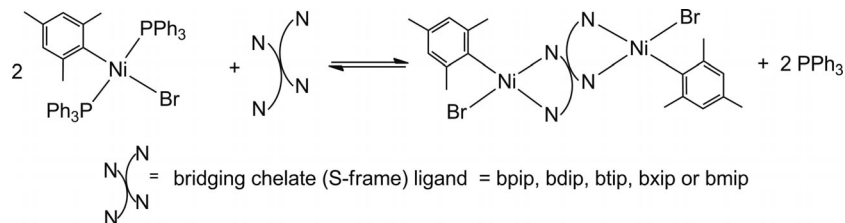
Scheme 1. Bridging diimine ligands used in this study. bpip = 2,5-bis(1-phenyliminoethyl)pyrazine, bdip = 2,5-bis[1-(3,5-dimethylphenyl)iminoethyl]pyrazine, btip = 2,5-bis[1-(2-methylphenyl)iminoethyl]pyrazine, bxip = 2,5-bis[1-(2,6-dimethylphenyl)iminoethyl]pyrazine and bmip = 2,5-bis[1-(2,4,6-trimethylphenyl)iminoethyl]pyrazine (including numbering of the pyrazine core). Indicated by [M] are the potential binding sites of metals.

ligand–metal interaction bpip and its derivatives are (bis-chelate) derivatives of 1,4-pyrazine and should thus combine high binding stability (chelate) with the excellent “bridging abilities” of 1,4-pyrazine, well established in the so-called “Creutz–Taube” ion.^[22] The variation of bpip to bdip, btip, bxip and bmip was motivated from the expected steric effects,^[21a] which play a very important role for example in the Brookhart-type ligands and is established as a pre-requisite for effective catalysts.^[1]

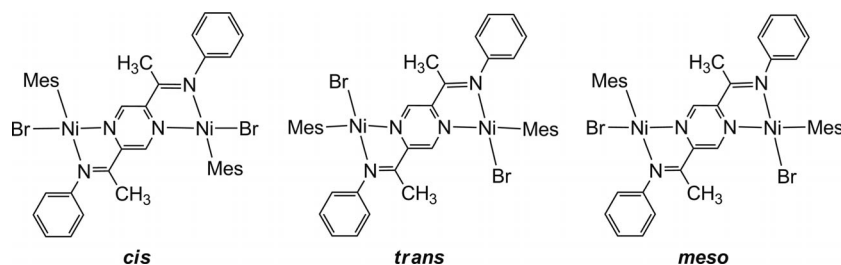
Results and Discussion

Synthesis and General Properties

The neutral complexes $[(\mu\text{-N}^{\wedge}\text{N})\{\text{Ni}(\text{Mes})\text{Br}\}_2]$ ($\text{N}^{\wedge}\text{N}$ = diimine ligands) were synthesised from the precursor complex *trans*- $[(\text{PPh}_3)_2\text{Ni}(\text{Mes})\text{Br}]$ by ligand exchange reactions



Scheme 2. Preparation of complexes $[(\mu\text{-N}^{\wedge}\text{N})\{\text{Ni}(\text{Mes})\text{Br}\}_2]$ from *trans*- $[(\text{PPh}_3)_2\text{Ni}(\text{Mes})\text{Br}]$ and the bridging ligands.



Scheme 3. Possible isomers for binuclear bromo mesityl nickel complexes.

in acetone or toluene solution (Scheme 2) and were analysed by ^1H NMR, ^{13}C NMR and elemental analysis (see Experimental Section).

In contrast to the recently reported mononuclear complexes $[(\text{N}^{\wedge}\text{N})\text{Ni}(\text{Mes})\text{Br}]$ with rather basic diimine ligands such as 2,2'-bipyridine (bpy)^[14,15] or the related binuclear bpm complex $[(\mu\text{-bpy})\{\text{Ni}(\text{Mes})\text{Br}\}_2]$ ^[16] for which the preparation reaction depicted in Scheme 2 proceeds very smoothly with high yield, for the less basic ligands bpip–bmip the preparation required thorough recrystallisation due to the presence of starting complex $[(\text{PPh}_3)_2\text{Ni}(\text{Mes})\text{Br}]$. From the very weakly basic but excellent acceptors 2,2'-azopyridine^[23] or bis(2-pyridyl)-3,4,5,6-tetrazine (bptz),^[24] no products were formed upon reaction with $[(\text{PPh}_3)_2\text{Ni}(\text{Mes})\text{Br}]$. Once formed and in the absence of PPh_3 or other strong ligands the new compounds are stable in solvents like CH_2Cl_2 , THF, toluene, acetone or even DMF towards ligand exchange reactions.^[15] The complexes undergo the same decomposition reaction as reported for the monomolecular analogues only in nitriles and alcohols.^[15,16,17] Examination of their thermal stability in the solid state by dynamic DSC (Differential Scanning Calorimetry) showed that the bxip and bmip derivatives are completely stable up to 205 °C, at which point they melt. Above 220 °C the complexes slowly decompose. In DMF solution the bmip derivative decomposed only upon prolonged (more than 8 h) heating above 152 °C (boiling) as investigated by NMR spectroscopy.

Complex ^1H NMR spectra were observed after short reaction times and rapid workup. Closer inspection, in part with the help of correlation methods, revealed that mixtures of isomers were present in these solutions. Scheme 3 depicts the three possible isomers for the bpip complex. However, the NMR experiments only show that there were two different orientations of the mesityl co-ligand, either *cis* to the aniline N atom (called the *cis* isomer) or *trans* to the pyrazine N atom (called the *trans* isomer). The depicted

meso isomer cannot be observed, but the signals might be coincident with those of the *cis* and *trans* isomers, thus the *meso* isomer cannot be ruled out. Leaving the reaction mixtures for a longer period of time or recrystallising the products several times yields pure spectra corresponding to the *cis* isomers. The complete spectral assignment of the isomers is given in the Experimental Section.

Structures

Unfortunately, none of the binuclear complexes could be obtained in the form of single crystals. A crystal structure was obtained from the new ligand bmip (details in the Supporting Information). Additionally, the structures of the free ligands, the one-electron reduced ligands and the binuclear [Ni(Mes)Br] complexes were calculated by DFT methods. The calculated geometries for the ligands are almost perfectly in line with the experimentally obtained (XRD) structures of the two ligands bmip and bpip.^[21b] We calculated the molecular structures of the binuclear nickel complexes in their *cis* isomeric form, and an example is shown in Figure 1. Tables 1, 2 and 3 list relevant structural parameters (full data in the Supporting Information).

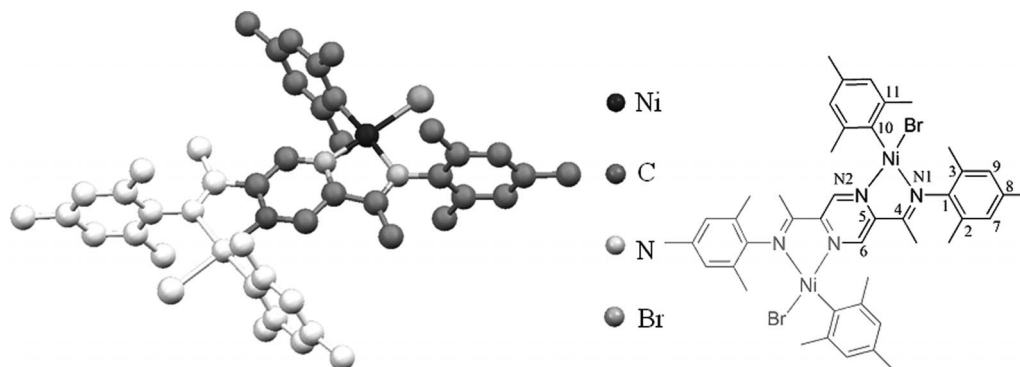


Figure 1. DFT-calculated molecular structure of *cis*-[(bmip){Ni(Mes)Br}₂] at the (RI-)BP86/SV(P) level of theory. Only one half of the centro-symmetric molecule was calculated.

Table 1. Essential DFT-calculated structural data of the free ligands at the (RI-)BP86/SV(P) level of theory.

	bpip ^[a]	bpip	bdip	btip	bxip	bmip	bmip ^[b]
Distances [Å]							
C(1)–N(1)	1.419(2)	1.3937	1.3952	1.3982	1.4024	1.4024	1.427(2)
C(4)–N(1)	1.279(2)	1.2912	1.2912	1.2911	1.2885	1.2881	1.273(2)
C(4)–C(5)	1.489(2)	1.5017	1.5006	1.5004	1.5032	1.5030	1.495(2)
C(5)–N(2)	1.336(2)	1.3497	1.3497	1.3498	1.3492	1.3494	1.338(2)
C(1)–C(2)	1.407(2)	1.4200	1.4292	1.4193	1.4248	1.4221	1.401(2)
Angles [°]							
C(2)–C(1)–N(1)	122.6(1)	122.6	122.4	122.3	120.3	120.9	119.4(1)
N(1)–C(4)–C(5)	116.0(1)	117.0	118.6	116.9	117.4	117.4	116.6(1)
N(2)–C(5)–C(4)	117.3(1)	118.3	118.3	118.3	118.2	118.2	117.7(1)
Dihedral angles [°]							
C(4)–N(1)–C(1)–C(2)	55.2(2)	60.0	58.9	55.9	81.5	79.9	82.5(1)
C(6)–C(5)–C(4)–N(1)	1.6(1)	0.5	3.7	0.6	2	3.1	6.2(1)

[a] X-ray diffraction data from ref.^[21b] [b] Data from X-ray diffraction (for details see Supporting Information).

Table 2. Essential DFT-calculated structural data of the ligand radical anions at the (RI-)BP86/SV(P) level of theory.

	[bpip] ^{•–}	[bdip] ^{•–}	[btip] ^{•–}	[bxip] ^{•–}	[bmip] ^{•–}
Distances [Å]					
C(1)–N(1)	1.3703	1.3719	1.3708	1.3786	1.3787
C(4)–N(1)	1.3200	1.3199	1.3202	1.3179	1.3175
C(4)–C(5)	1.4576	1.4582	1.4569	1.4559	1.4557
C(5)–N(2)	1.3790	1.3798	1.3792	1.3818	1.3820
C(1)–C(2)	1.4324	1.4282	1.4297	1.4364	1.4329
Angles [°]					
C(2)–C(1)–N(1)	126.4	123.9	127.2	126.1	126.7
N(1)–C(4)–C(5)	119.3	119.4	119.2	119.9	119.9
N(2)–C(5)–C(4)	119.1	119.0	119.1	118.8	118.9
Dihedral angle [°]					
C(4)–N(1)–C(1)–C(2)	49.0	48.7	46.5	77.9	76.2

Both the free ligands and the binuclear complexes reveal an essentially co-planar arrangement of the central pyrazine and the 2,5-substituted iminoethyl group (the largest tilt angle is 6.2° for bmip). In the complexes the nickel atoms were located quite perfectly in this plane thus showing perfect square-planar coordination (see Table 3). Compared to this

Table 3. Essential DFT-calculated structural data of $[(\mu\text{-bmip})\{\text{Ni}(\text{Mes})\text{Br}\}_2]$ and $[(\mu\text{-bpip})\{\text{Ni}(\text{Mes})\text{Br}\}_2]$ at the (RI)-BP86/SV(P) level of theory.

<i>cis</i> - $[(\mu\text{-L})\{\text{Ni}(\text{Mes})\text{Br}\}_2]$			<i>trans</i> - $[(\mu\text{-L})\{\text{Ni}(\text{Mes})\text{Br}\}_2]$		
Distances [Å]	(bmip)	(bpip)		(bmip)	(bpip)
Ni(1)–N(1)	2.009	2.016	Ni(1)–N(1)	1.921	1.906
Ni(1)–N(2)	1.897	1.888	Ni(1)–N(2)	1.975	1.983
Ni(1)–C(10)	1.901	1.901	Ni(1)–C(10)	1.911	1.902
Ni(1)–Br(1)	2.290	2.287	Ni(1)–Br(1)	2.301	2.297
Angles [°]					
N(1)–Ni(1)–N(2)	82.4	82.1	N(1)–Ni(1)–N(2)	82.1	82.2
N(2)–Ni(1)–C(10)	93.3	93.1	N(2)–Ni(1)–Br(1)	96.2	95.6
C(10)–Ni(1)–Br(1)	87.4	86.5	Br(1)–Ni(1)–C(10)	87.6	87.1
Br(1)–Ni(1)–N(1)	96.9	98.1	C(10)–Ni(1)–N(1)	97.7	95.4
N(1)–Ni(1)–C(10)	175.7	175.1	N(1)–Ni(1)–Br(1)	167.9	175.0
N(2)–Ni(1)–Br(1)	179.2	179.6	N(2)–Ni(1)–C(10)	161.5	173.8
Sum of angles [°]	360.0	359.8	sum of angles [°]	363.6	360.3
Dihedral angles [°]					
C(4)–N(1)–C(1)–C(2)	91.5	66.2	C(4)–N(1)–C(1)–C(2)	82.4	71.9
N(1)–Ni(1)–C(10)–C(11)	82.9	99.3	N(1)–Ni(1)–C(10)–C(11)	83.9	90.9
C(6)–C(5)–C(4)–N(1)	179.9	179.3	C(6)–C(5)–C(4)–N(1)	173.2	177.5

plane the “aniline group” of the ligand scaffold and the aryl co-ligand at the nickel atom are markedly tilted. The latter tilt angles are about 83° for the bmip derivative, while the bpip complex shows 81 or 90°. Related mononuclear dimesityl nickel or dimesityl platinum complexes revealed rather invariant tilt angles of about 70°. [15] The tilt angle of the aniline group in the two complexes depends strongly on the substituents and it has been proposed that the electron density on the imino N atom (and thus a number of properties) is determined by this tilt angle. [21] Thus, while for steric reasons a tilt angle of 90° would be preferable, deviations from 90° indicate an electronic interaction of the aromatic substituent with the aromatic scaffold of the ligand. Structural and theoretical studies on the ligand bpip (tilt angle 54.9°) and the Cu^I complex $[(\mu\text{-bpip})\{\text{Cu}(\text{PPh}_3)_2\}_2](\text{BF}_4)_2$ (tilt angle 89.3°) have revealed an interaction between the phenyl orbitals and π -orbitals of the binding plane. [21b] While the tilt angle in the free ligand bpip provides a perfect angle for this interaction, steric restraints from the (phosphane) co-ligands force the angle to almost 90° in the copper bpip complex, thus minimising the interaction. Furthermore, it can be expected that *ortho*-substitution on the aniline groups will increase the steric restraints (repulsion of the *ortho* groups and the iminoethyl group of the ligand and co-ligands on the metal) and might also lead to tilt angles around 90° thus minimising the steric repulsion but at the same time the aniline-binding plane interaction.

Our calculations show that the dihedral angles between the binding plane and the aniline group fall into two groups for the ligands (Table 1). The first group exhibits angles roughly around 60° and contains all ligands with non-bulky aniline groups. Interestingly, this includes the 2-tolyl derivative btip. The second group showing an angle of about 80° is formed by bxip and bmip, both with a 2,6-dimethyl substitution pattern. The same groups are observed for the structures of the one-electron reduced ligands (Table 2). For these species the tilt angle is markedly decreased for the first

group, thus supporting the assumed interaction (extension of the pyrazine π -system is favourable for the reduced species). Additionally, the calculated geometrical changes in the ligand scaffold upon one-electron addition (presumably to the π^* -orbital) are in line with the expected change of the character of the central pyrazine core from aromatic 1,4-pyrazine towards a *p*-benzoquinone diimine structure. Importantly, these changes extend into the aniline groups [e.g. C(1)–N(1) and C(1)–C(2) in Table 2]. Coordination of two $[\text{Ni}(\text{Mes})\text{Br}]$ fragments leads to an almost perpendicular arrangement of both the aniline group and the mesityl co-ligands towards the coordination plane in the binuclear bmip complex (exhibiting higher steric strain), while the tilt angle of the aniline group is markedly lower for the bpip derivative. In this case it is obvious that lower steric strain allows an electronically favourable orientation of the aniline group. Support for the assumed electronic interaction between the binding plane and the aniline groups has to come from electrochemistry and spectroscopy in solution.

In addition to the structural parameters, we also calculated the energy difference between the *cis* and *trans* isomers for the binuclear complexes of bpip and the highest substituted ligand bmip. In the case of bpip the *cis* isomer was found to be 4.41 kJ mol^{−1} (ΔG) lower in energy, hence more stable, than the *trans* isomer. As expected, the energy difference between both isomers of the sterically bulky ligand bmip is significantly higher. The *cis* isomer is 25.4 kJ mol^{−1} lower in energy than the *trans* isomer.

Electrochemistry

The electrochemistry of the free ligands (see data in the Supporting Information) and nickel complexes was studied using cyclic and square-wave voltammetry. The cyclic voltammograms of all complexes in THF solution, as exemplified in Figure 2 (top), show two reversible one-electron

reductions. Comparison with other transition-metal complexes of these ligands suggest ligand-centred reductions.^[19–21] Remarkably, the anodic shift for the first reduction wave for the free ligands and the binuclear nickel complexes accounts for more than one Volt. Further reduction waves are irreversible. In the anodic area broad irreversible oxidation waves were observed, which account for two electrons. On the basis of similar results from mononuclear derivatives, we assign them to metal-centred oxidations Ni^{II}/Ni^{III} for the two nickel atoms.^[17,18] From the voltammetry there is no evidence that the two oxidation events are separated due to electronic coupling of the metal centres, which would allow generation of an intermediate mixed-valent state. Thus, the highest occupied molecular orbital in these complexes (HOMO) is rather localised on the Ni^{II} (d⁸) centres, in line with similar observations for Ru^{II}, Rh^{III} or Ir^{III} bpip complexes (Table 4).^[21,22]

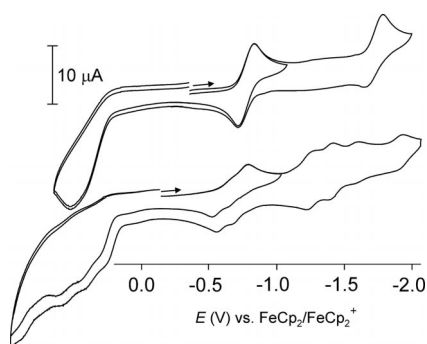


Figure 2. Cyclic voltammograms of [(bmip){Ni(Mes)Br}₂] in THF/*n*Bu₄NPF₆ (top), and in DMF/*n*Bu₄NPF₆ solution (bottom), measurements at 298 K and 100 mV s⁻¹ scan rate.

Table 4. Selected electrochemical data of binuclear complexes [(μ-N^{^N}){Ni(Mes)Br}₂].^[a,b]

N ^{^N}	<i>E</i> _{pa} Ox1	<i>E</i> _{1/2} Red1 (Δ <i>E</i> _{pp})	<i>E</i> _{1/2} Red2 (Δ <i>E</i> _{pp})	<i>E</i> _{pc} Red3	Solvent/ <i>T</i>
bpip	0.30	-0.78 (75)	-1.60 (78)	-1.97	THF/r.t.
bdip	0.34	-0.84 (68)	-1.66 (90)	-2.05	THF/r.t.
btip	0.33	-0.78 (78)	-1.66 (92)	-2.02	THF/r.t.
bxip	0.34	-0.82 (60)	-1.73 (66)	-3.07	THF/r.t.
bmip	0.41	-0.82 (70)	-1.68 (90)	-2.11	THF/r.t.
bpip	0.29	-0.76 (75)	-1.58 (78)	-1.93	DMF/r.t.
bpip	0.40	-0.77 (70)	-1.48 (71)	–	DMF/-60 °C
bmip	(1) 0.29	-0.55 (75)	-1.26 (91)	-1.93	DMF/r.t.
	(2)	-0.65 (75)	-1.39 (78)	–	
	(3)	-0.76 (75)	-1.57 (75)	–	
bmip	(1) 0.41	-0.55 (74)	-1.32 (71)	-1.90	DMF/-60 °C
	(2)	-0.69 (74)	-1.48 (81)	–	
	(3)	-0.78 (74)	–	–	

[a] The measurements were performed on the pure *cis* isomers of the complexes. [b] Potentials from cyclic or square wave voltammetry in 0.1-M *n*Bu₄NPF₆/solvent solutions (in V) vs. ferrocene/ferrocenium. Half-wave potentials *E*_{1/2} given with *peak-to-peak* separation Δ*E*_{pp} in parentheses (in mV) for reversible processes; cathodic *E*_{pc}, or anodic *E*_{pa} peak potentials for irreversible processes.

While the cyclic voltammograms of the bpip complex in DMF solution differ only marginally from those in THF solution, the bdip, btip, bxip, and bmip derivatives exhibit

apparently completely different reduction behaviour in DMF solution (Figure 2, bottom). Instead of two reduction waves (as in THF) we can see two packages of several waves. Each of these packages contains one electron and all these processes are completely reversible. Using square-wave voltammetry (Figure 3), the complex features can be resolved into three waves [entries (1) to (3)]. The thus-obtained 2 × 3 potentials are listed in Table 2 for the bmip complex. At higher scan rates (up to 5 V s⁻¹) and/or at lower temperatures the situation remains largely the same, only the third wave [entry (3)] of each package gains some intensity, while the other two decrease slightly. The oxidation waves in DMF solution look essentially the same as for the measurements in THF. Importantly, this behaviour is observed for both isomeric mixtures as well as for materials containing the pure *cis* isomers.

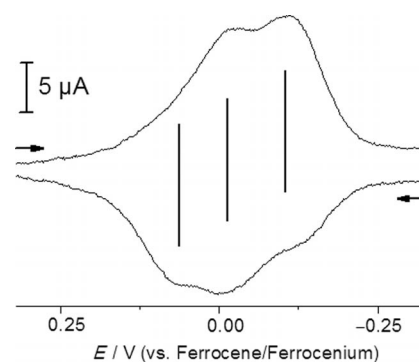
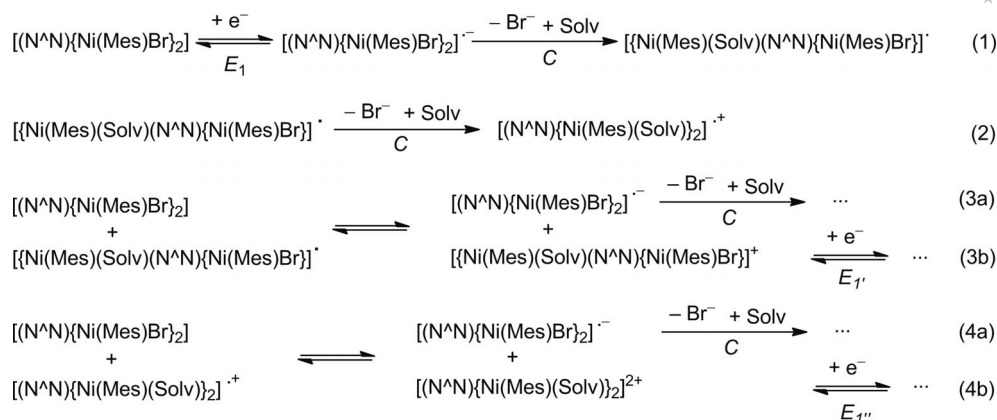


Figure 3. Square-wave voltammetry of [(μ-bmip){Ni(Mes)Br}₂] in DMF/*n*Bu₄NPF₆ solution, measurements at 298 K and 20 mV s⁻¹ scan rate showing both an anodic and a cathodic scan of the first reduction. The three bars represent the three obtained potentials.

The peculiar behaviour of these complexes in DMF solution might be explained by the partial splitting of the bromido ligand from the parent compounds or by the presence of isomers. However, for the detailed electrochemical measurements carried out on these two complexes we used the pure *cis* isomers and from ¹H NMR measurements in DMF we have no indication that isomerisation in this solvent occurs to a large extent. A comparison of the reduction potentials of the bpip complex in THF or DMF solution reveals no marked dependence of the potentials on the solvent polarity. If this holds also for the other derivatives, the third wave (3) of each package should correspond to the reduction of the parent complexes *cis*-[(μ-N^{^N}){Ni(Mes)Br}₂], which is supported by fast-scan and low-temperature experiments. From this we can conclude that the species responsible for the complicated plots exhibit slightly less negative reduction potentials than the parent complexes (or isomers). For the *trans* isomer and the possible *meso* isomer (if present – see NMR) we would, however, expect more negative values, because of the electron-donating character of the mesityl co-ligand in *trans* position to the main reduction target, which is most probably the pyrazine core (see EPR spectroscopy below). Additionally, for the related complex [(μ-bpym){Ni(Mes)Br}₂] no differences in the reduction behaviour for the two isomers (*cis* and *trans*) was



Scheme 4. Schematic representation of the assumed electron transfer-induced solvolysis reaction.

observed.^[16] Therefore, we can very probably discard the possibility of isomerisation being responsible for the peculiar behaviour. Conversely, it was previously established, that the one-electron reduced mononuclear complexes $[(\text{N}^{\wedge}\text{N})\text{Ni}(\text{Mes})\text{Br}]^{-\cdot}$ readily cleave the Br co-ligand (as bromide),^[6,18] and the resulting complexes $[(\text{N}^{\wedge}\text{N})\text{Ni}(\text{Mes})(\text{Solv})]$ (Solv = solvent molecule) exhibit re-oxidation potentials anodically shifted by approx. 0.3 V compared to the neutral precursor complexes. We thus carried out corresponding experiments and could show that upon addition of $n\text{Bu}_4\text{NBr}$ or upon applying low temperatures the splitting process can be slowed down (see Supporting Information).^[18] Therefore, we assume partially dehalogenated species $[\{\text{Ni}(\text{Mes})\text{Br}\}(\mu\text{-N}^{\wedge}\text{N})\{\text{Ni}(\text{Mes})(\text{Solv})\}]^{\cdot+}$ or $[(\mu\text{-N}^{\wedge}\text{N})\{\text{Ni}(\text{Mes})(\text{Solv})\}_2]^{2+\cdot}$ to account for the minor waves at slightly higher potentials [packages (1) and (2)]. Since from ^1H NMR spectroscopy of the parent complexes we have no evidence for such solvolysis, we might assume, that they are formed by an electron transfer-induced solvolysis reaction (Scheme 4).^[25]

Provided the solvolysis reaction *C* occurs very quickly [see Equations (1) and (2) in Scheme 4] the resulting radical complexes $[\{\text{Ni}(\text{Mes})\text{Br}\}(\mu\text{-N}^{\wedge}\text{N})\{\text{Ni}(\text{Mes})(\text{Solv})\}]^{\cdot+}$ ($n = 0, 1$) might reduce the parent complex [see parts a of Equations (3) and (4)], while forming the cationic solvent complexes $[\{\text{Ni}(\text{Mes})\text{Br}\}(\mu\text{-N}^{\wedge}\text{N})\{\text{Ni}(\text{Mes})(\text{Solv})\}]^{m+}$ ($m = 1$ or 2), which have less negative reduction potentials ($E_{1'}$ or $E_{1''}$) than the parent complex (E_1) [see parts b of Equations (3) and (4)]. Hence, although only a very small fraction of the parent complex is reduced at potentials $E > E_1$, an appreciable amount of cationic complexes could be formed. The assumed mechanism is strongly supported by the square-wave voltammogram shown in Figure 3. The anodic scan starting from -0.3 V exhibits a far larger amount of the species responsible for the highest potential (presumably the dicationic solvent complex), than observed for the cathodic scan (starting from 0.3 V). Interestingly, the electrochemical behaviour of bpip is thus different to the rest of the series, the bdip, btip, bxip derivatives all strongly resemble the bmip complex. Since the electrochemical potentials for the first and second reduction do not differ markedly within our series of complexes we can state that the

overall electronic structure of the complexes is essentially the same. The observed lability in DMF solution is ascribed to a loss of Br^- from the reduced complexes, a reaction which seems to be slow for the bpip complex and is accelerated for derivatives with methyl-substituted aniline groups. Since a straight correlation with observed structural parameters, especially the tilt angle between the coordination plane and the aniline group and the electrochemical data cannot be drawn, we might also assume, that the electron-donating nature of the methyl substituents generally favours the cleavage of the Br^- ligand, although a clear correlation of the number of substituents with the reduction potentials also fails. In any case a marked difference between the bpip complex and the other derivatives has been found.

Absorption Spectroscopy

The binuclear complexes all exhibit a bright green colour in the solid as well as in solution. The absorption spectra (Figure 4) are dominated by two broad bands of medium intensity in the visible region and intense bands in the UV region. The two broad bands in the visible show negative

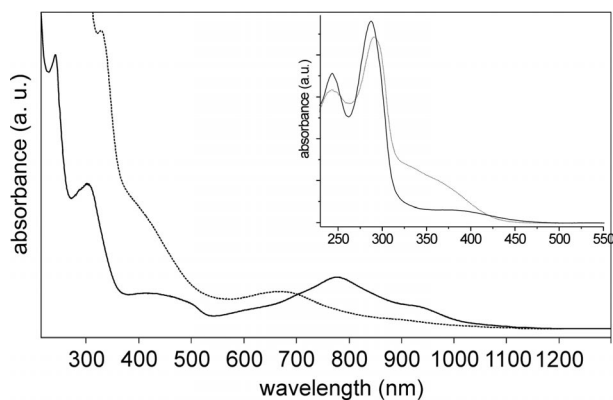


Figure 4. Absorption spectra of $[(\mu\text{-bmip})\{\text{Ni}(\text{Mes})\text{Br}\}_2]$ (—) and $[(\mu\text{-bpip})\{\text{Ni}(\text{Mes})\text{Br}\}_2]$ (----) in CH_2Cl_2 solution (the insert shows the spectra of the free ligands bmip and bpip measured in CH_2Cl_2 solution).

Table 5. Absorption maxima of binuclear nickel complexes $[(N^{\wedge}N)\{Ni(Mes)Br\}_2]$.^[a]

$N^{\wedge}N$	λ [nm]			
bpip	292 (32), 327 sh (18)	401 sh (15.0)	674 (5.5)	912 sh (3.1)
bdip	256 (30), 307 (21)	424 (7.6), 481 sh (4.1)	771 (10.8)	923 sh (3.5)
btip	284 (27), 323 sh (17)	435 (7.3), 491 sh (6.4)	782 (17.4)	928 (9.4)
bxip	237 (32), 291 (19)	432 sh (3.8), 494 (4.1)	784 (10.5)	936 (5.8)
bmip	239 (37), 304 (20)	430 sh (4.0), 494 (4.8)	783 (11.0)	930 (6.1)

[a] Absorption maxima λ in nm as measured in CH_2Cl_2 solution, main maxima are underlined, extinction coefficients ϵ in $1000\text{ M}^{-1}\text{ cm}^{-1}$ are given in parentheses.

solvatochromism (spectra in the Supporting Information), while the UV bands are solvent invariant.

On the basis of the band intensities, the observed solvatochromism and studies of related mononuclear complexes^[15b] we can assign the bands at high energy to ligand-centred (π - π^*) transitions, while the two long-wavelength band systems result from metal-to-ligand charge-transfer (MLCT) transitions (data in Table 5). The very low energy of the latter can be attributed to a marked electronic coupling of the two metal centres over the ligand bridge via their low-lying π^* orbitals.^[21]

A closer look reveals that the dominant MLCT bands are around 780 nm for the bmip, btip and bxip complexes. Slightly higher energies are found for the bdip and markedly higher energies for the bpip complex. The same is true for the very low energy maxima at around 920 nm and the high-energy MLCT bands at around 420 nm. Also in the UV region the spectrum for the bpip complex reveals marked differences to the other derivatives. Remarkably also the spectra of the uncoordinated ligands exhibit qualitatively the same differences (Figure 4 inset), which thus can be traced to the different aniline groups (full spectroscopic data of the ligands in the Supporting Information).

The free ligand btip and the corresponding nickel complex $[(btip)\{Ni(Mes)Br\}_2]$ have been submitted to spectroelectrochemical experiments examining the two reversible reduction waves (Figure 5). During the first reduction step the broad MLCT band vanishes leaving some residual ab-

sorption at 750 nm. In the visible, two intense and partially structured bands rise with maxima at 381 and 589 nm (Table 6).

Table 6. Spectroelectrochemical data of btip and $[(\mu\text{-btip})\{Ni(Mes)Br\}_2]$.^[a]

	λ [nm]				
$[(btip)\{Ni(Mes)Br\}_2]$	272	420	480 sh	767	902 sh
$[(btip)\{Ni(Mes)Br\}_2]^-$	246	<u>381</u>	589	740	887 sh
$[(btip)\{Ni(Mes)Br\}_2]^{2-}$	246	320 sh	360 sh	<u>549</u>	
btip	291	294	330 sh	365 sh	
$[btip]^-$	280	460 sh	480	720	885 sh
$[btip]^{2-}$	276	328 sh sh	360 sh	<u>479</u>	

[a] Electrolysed in situ in an OTTLE cell in THF/*n*Bu₄PF₆; absorption maxima λ in nm, main maxima are underlined.

The second reduction leads essentially to a blue-shift of the two visible bands and an increase in intensity. For the free ligand essentially the same spectroscopic changes were observed during reductive electrolysis (Table 6) and similar absorptions have been observed for reduced bpip complexes of $[Re(CO)_3Cl]$ or $[M(C_5Me_5)Cl]$ ($M = Ir$ or Rh).^[19b,20a] Thus, the two reductions of the nickel complexes $[(\mu\text{-}N^{\wedge}N)\{Ni(Mes)Br\}_2]$ can be assigned to essentially ligand-based processes; the stepwise reduction leads to blue-shifting and bleaching of the MLCT bands and the appearance of additional π - π^* absorption in the reduced ligands $(N^{\wedge}N)^-$ and $(N^{\wedge}N)^{2-}$.

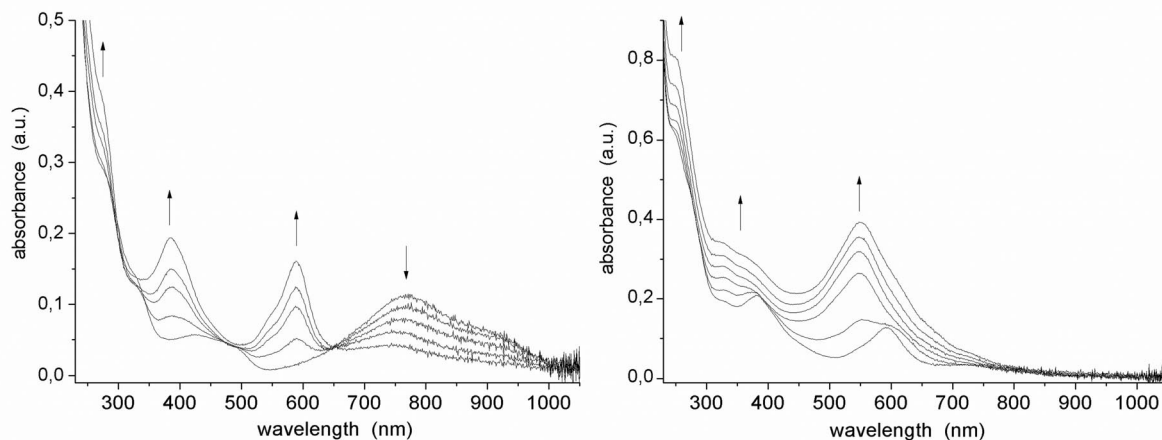


Figure 5. Absorption spectra of $[(\mu\text{-btip})\{Ni(Mes)Br\}_2]$ recorded during in situ electrolysis in THF/*n*Bu₄NPF₆ at 298 K; left: during first reduction, right: during second reduction.

EPR Spectroscopy

EPR spectra have been recorded on electrochemically generated radical anions of the binuclear nickel complexes at 298 K in fluid solution and in glassy frozen solutions at 110 K. Furthermore, the reduced ligand bxip^- and the radical anion generated from the precursor molecule 2,5-diacyetyl-1,4-pyrazine (dapz) were investigated. Figure 6 shows representative examples and Table 7 summarises the data. From Figure 6 we can see, that the signal for the free ligand radical anion bxip^- exhibits hyperfine splitting (hfs), the same is true for dapz and the previously reported bpip^- .^[26] From spectral simulation of all three species we can conclude that the hfs is due to the coupling to the pyrazine N atoms, the imino N atom, the iminoethyl H and the pyrazine H atoms. Comparison of the coupling constants reveals a re-distribution of the spin density within the series dapz^- , bpip^- and bxip^- . The observed differences between bpip and bxip are completely in line with the DFT-calculated spin densities (Supporting Information). Increasing substitution on the aniline group decreases the (re)distribution of spin density over the entire molecule (up to the aniline group), thus increasing the density in the central pyrazine-imine entity (with the consequence of increased coupling constants).

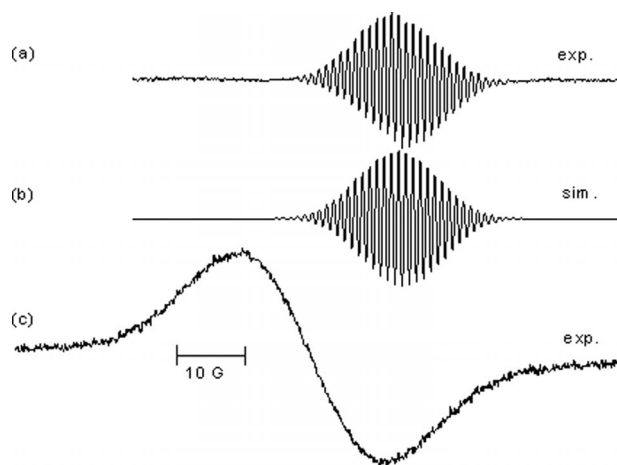


Figure 6. X-band EPR spectra of $(\text{bxip})^-$ (a) with spectral simulation (b) and $[(\mu\text{-bxip})\{\text{Ni}(\text{Mes})\text{Br}\}_2]^-$ (c) recorded during in situ electrolysis in $\text{THF}/n\text{Bu}_4\text{NPF}_6$ at 298 K.

For the binuclear nickel complex $[(\mu\text{-N}^{\wedge}\text{N})\{\text{Ni}(\text{Mes})\text{Br}\}_2]^-$ (generated by electrolysis) we obtained unresolved isotropic EPR signals at 298 K in fluid solution centred at around $g = 2.02$ (Figure 6). In contrast to this, the radical anions $[(\mu\text{-bpym})\{\text{Ni}(\text{Mes})\text{Br}\}_2]^-$ and $[(\text{bpym})\text{Ni}(\text{Mes})\text{Br}]^-$ gave well-resolved EPR spectra.^[16]

In glassy frozen solutions at 110 K anisotropic spectra of rhombic symmetry were observed with averaged g_{av} values identical to the isotropic signals (g_{iso}) at 298 K thus confirming that the same species were observed (Figures in the Supporting Information). Unfortunately the signals were completely unresolved. Nevertheless, from the $g_{\text{iso}} = g_{\text{av}}$ values not far above the value of the free electron $g_e = 2.0023$

Table 7. EPR data of radical anionic ligands $(\text{N}^{\wedge}\text{N})^-$, $(\text{dapz})^-$ and reduced nickel complexes.^[a]

Radical	g_{iso}	$a_{\text{N-pyz}}$	$a_{\text{N-imin}}$	$a_{\text{H-methyl}}$	$a_{\text{H-pyz}}$
$(\text{dapz})^-$	2.005	0.173	–	0.173	0.173
$(\text{bpip})^-$ ^[b]	2.003	0.159	0.159	0.186	0.018
$(\text{bxip})^-$	2.003	0.323	0.323	0.200	0.170

$[(\text{N}^{\wedge}\text{N})\{\text{Ni}(\text{Mes})\text{Br}\}_2]^-$	g_{iso}	g_{av}	g_1	g_2	g_3	Δg
bpip	2.0180	2.0180	2.0353	2.0183	2.0004	0.0349
bdip	2.0186	2.0186	2.0359	2.0146	2.0053	0.0306
btip	2.0180	2.0180	2.0456	2.0120	1.9965	0.0491
bxip	2.0187	2.0187	2.0503	2.0117	1.9942	0.0561
bmip	2.0182	2.0183	2.0515	2.0143	1.9891	0.0622

[a] Radical species generated in situ by electrolysis in $\text{THF}/n\text{Bu}_4\text{NPF}_6$ at ambient temperature. Coupling constants a_{X} and isotropic g values g_{iso} from spectral simulation in mT ($1 T = 10^4 G$) from measurements at 298 K. Averaged g values $g_{\text{av}} = (g_1 + g_2 + g_3)/3$ and g anisotropy $\Delta g = g_1 - g_3$ from measurements at 110 K. [b] From ref.^[26]

and the rather small g anisotropy Δg we can conclude that the singly occupied molecular orbitals (SOMOs) in these complexes are mainly centred on the organic bridging ligand with only very small contributions from the nickel atoms.

Thus, the radical complexes can be described as $[\text{Ni}^{\text{II}}(\text{Mes})\text{Br}]$ complex fragments coordinated to $(\mu\text{-N}^{\wedge}\text{N})^-$ radical bridging ligands, in line with the UV/Vis spectroelectrochemical experiments. Compared to the above-mentioned complexes $[(\mu\text{-bpym})\{\text{Ni}(\text{Mes})\text{Br}\}_2]^-$ and $[(\text{bpym})\text{Ni}(\text{Mes})\text{Br}]^-$ both the g_{iso} (ca. 2.004) and Δg (ca. 0.025) values are slightly increased pointing to slightly increased nickel contributions, however, for radical complexes with a marked nickel contribution to the SOMO (in the sense of Ni^{I} complexes) far higher g values (>2.1) and Δg (>0.1) were observed.^[27]

Catalytic Negishi Cross-Coupling Reactions

With the binuclear complexes in hand, we wanted to demonstrate the proof-in-principle that such frameworks can support catalytic reactions of current interest. Nickel has been especially useful in the cross-coupling of aryl halides with alkylzinc nucleophiles to generate new $\text{C}(sp^2)\text{-C}(sp^3)$ bonds.^[8c] Table 8 describes our initial results using the binuclear complexes based on the bxip and btip ligands in comparison with the recently reported binuclear complex $[(\text{bpym})\{\text{Ni}(\text{Mes})\text{Br}\}_2]$.^[16]

Gratifyingly, all three complexes were able to catalytically mediate the Negishi reaction described in Table 8 under mild room temperature conditions, with the bpym complex affording the highest yield of product. No side products resulting from β -hydride eliminations were detected in the GC–MS.

Interestingly, the complexes displayed higher reactivity with the functionalised 2-(1,3-dioxan-2-yl)ethylzinc bromide than the non-functionalised pentylzinc bromide. While the yields are moderate and not yet competitive with the

Table 8. Activity of selected binuclear complexes for aryl–alkyl cross-coupling reactions.^[a]

Ar-I + R_{alkyl}-ZnX $\xrightarrow[THF, 25\text{ }^\circ\text{C}]{2.5\text{ mol-\%}}$ Ar-R_{alkyl}

Entry	Aryl iodide	Alkylzinc reagent	Product	% Yield, ligand	Time [h]
1				19, bxip	92
				56, btip	92
				63, bpym	4.5
2				47, bxip	92
				56, btip	24
				68, bpym	4.5
3				13, bxip	2
				17, btip	92
				51, bpym	4.5
4				13, bxip	2
				11, btip	12
				36, bpym	4.5

[a] All yields based on GC analyses relative to a calibrated internal standard.

use of bipyridine nickel catalysts,^[8c] the results do show that the binuclear complexes can indeed carry out synthetic transformations that have been historically quite difficult.

Conclusions

The binuclear organometallic nickel complexes $[(\mu\text{-N}^{\wedge}\text{N})\{\text{Ni}(\text{Mes})\text{Br}\}_2] \{\text{N}^{\wedge}\text{N} = 2,5\text{-bis}[1\text{-(aryl)iminoethyl}]\text{pyrazine with aryl} = \text{phenyl, 2-tolyl, 2,6-xylyl, 3,5-xylyl and mesityl; Mes} = \text{mesityl} = 2,4,6\text{-trimethylphenyl}\}$ were prepared and characterised electrochemically and spectroscopically in detail. A combination of NMR spectroscopy and quantum chemical calculations gave a reasonable picture of the molecular structures and also showed that the *cis* configuration of the complexes is more stable. The complexes exhibit very long wavelength absorptions (600–1000 nm) which can be assigned to metal-to-ligand charge-transfer transitions. The very low energy of them (1.2–2 eV) is ascribed to a marked electronic coupling of the two metal centres over the ligand bridge via the low-lying π^* orbitals. In contrast to this, in voltammetric experiments no coupling of the two nickel-centred irreversible oxidations $\text{Ni}^{\text{II}}/\text{Ni}^{\text{III}}$ was observed. The reversible reductive electrochemistry yields stable radical anionic complexes with mainly ligand-centred spin density as shown by EPR spectroscopy, UV/Vis spectroelectrochemistry and DFT calculations. The

singly occupied molecular orbital (SOMO) is delocalised over the entire π -system of the ligand, including the N- and α -C atom of the aniline substituent. Since these substituents are involved in repulsive interaction with the mesityl co-ligands on the nickel atom the tilt angle of the aniline substituent does not allow further delocalisation. As inferred from the *g* values and the small *g* anisotropy of the EPR spectra at low temperature, the contribution of nickel to the SOMO is small thus, the complexes are best described as $[\text{Ni}^{\text{II}}(\text{Mes})\text{Br}]$ fragments coordinating to radical anionic bridging ligands $(\mu\text{-N}^{\wedge}\text{N})^{\cdot-}$. Interestingly, while the aryl = phenyl derivative shows two well-defined reduction waves in cyclovoltammetric measurements, the complexes carrying more sterically demanding substituents such as tolyl, xylyl or mesityl exhibit a complex behaviour in DMF solution. It is assumed that this polar solvent is able to partly replace the bromido ligand thus leading to minor amounts of solvent complexes. The latter are probably interesting candidates for nickel-based (electro)catalytical C–C coupling reactions. Preliminary Negishi cross-coupling reactions show that the complexes are moderately active. Future work will focus on whether the binuclear systems are inherently more stable than mononuclear derivatives (from our preliminary experiments we cannot draw an unequivocal conclusion on this), on whether their reactivity can be increased by addition of polar solvents (Br-splitting), and on determination of the background of the observed higher reactivity with the functionalised 2-(1,3-dioxan-2-yl)ethylzinc bromide.

Experimental Section

Instrumentation: Elemental analyses were obtained with a HEKAtech CHNS EuroEA 3000 analyser. NMR spectra were recorded with Bruker Avance II 300 MHz (^1H : 300.13 MHz, ^{13}C : 75.47 MHz) or Bruker Avance 400 MHz (^1H : 400.13 MHz, ^{13}C : 100.61 MHz) spectrometers, using a triple-resonance $^1\text{H}/^{19}\text{F}/\text{BB}$ inverse probe head. The unambiguous assignment of the ^1H and ^{13}C resonances was obtained from ^1H TOCSY, ^1H COSY, gradient-selected ^1H , ^{13}C HSQC and HMBC experiments. All 2D NMR experiments were performed using standard pulse sequences from the Bruker pulse program library. Chemical shifts were relative to Tetramethylsilane (TMS). Spectra were evaluated with Bruker TopSpin2. UV/Vis/NIR absorption spectra were recorded with Varian Cary 05E or Cary50 Scan spectrophotometers. Electrochemical experiments were carried out in 0.1-M $n\text{Bu}_4\text{NPF}_6$ solutions using a three-electrode configuration (glassy carbon electrode, Pt counter electrode, Ag/AgCl reference) and an Autolab PGSTAT30 potentiostat and function generator. The ferrocene/ferrocenium couple served as the internal reference. UV/Vis spectroelectrochemical measurements were performed with an optical transparent thin-layer electrochemical (OTTLE) cell.^[28] EPR spectra were recorded in the X-band with a Bruker System ELEXSYS 500E, using a Bruker Variable Temperature Unit ER 4131VT. g values were calibrated using a dpph sample. Spectral simulation was performed using Bruker SimFonia V1.26 or P.E.S.T. WinSim free software v. 0.96 (National Institute of Environmental Health Sciences). Dynamic DSC was measured with a Netzsch DTA404 PC under argon.

Crystal Structure Analysis for bmip: Data collection was performed at $T = 173(2)$ K on a Siemens P4 diffractometer with Mo- K_α radiation ($\lambda = 0.71073$ Å). The structure was solved by direct methods using the SHELXTL-PLUS package^[29] and refinement was carried out with SHELXL 97 employing full-matrix least-squares methods on F^2 with $F_0^2 \geq -2\sigma(F_0^2)$. Empirical absorption correction was performed using Ψ -scans. All non-hydrogen atoms were treated anisotropically; hydrogen atoms were found from the Fourier map and refined.

CCDC-853102 contains the crystallographic data for bmip. These data can be obtained free of charge from The Cambridge Crystallographic Data Centre via www.ccdc.cam.ac.uk/data_request/cif.

Quantum Chemical Calculation: All calculations were performed using density functional theory as implemented in the Turbomole 6.3^[30] package using the resolution of identity (RI) approximation.^[31–33] The geometry optimisations were performed at the (RI)-BP86/SV(P) level. All minima were confirmed as such by the absence of imaginary frequencies. The agreement between experimentally determined and calculated structures of the ligands bpip and bmip was very good. For the geometry and energy of the binuclear complexes only half of the centro-symmetric *cis* and *trans* isomers were calculated.

Materials and Procedures: The precursor complex $[(\text{PPh}_3)_2\text{Ni}(\text{Mes})\text{Br}]^{[13,14]}$ and the ligand bpip^[26] were obtained following literature procedures. The ligands bpip, bdip, btip, bxip and bmip were prepared in an analogous way as the xylyl derivative.^[21a] bdip: ^1H NMR ($[\text{D}_6]\text{acetone}$): $\delta = 9.41$ (s, 2 H, pz-H), 6.80 (s, 2 H, *p*-H), 6.52 (s, 4 H, *o*-H), 2.36 (s, 6 H, CH_3imin), 2.32 (s, 12 H, CH_3) ppm. btip: ^1H NMR ($[\text{D}_1]\text{chloroform}$): $\delta = 9.56$ (s, 2 H, pz-H), 7.25 (m, 4 H, *m*-H), 7.09 (t, 2 H, *p*-H), 6.73 (dd, 2 H, *o*-H), 2.35 (s, 6 H, CH_3imine), 2.17 (s, 6 H, ToICH_3) ppm. bxip: ^1H NMR ($[\text{D}_6]\text{acetone}$): $\delta = 9.17$ (s, 2 H, pz-H), 6.82 (d, 4 H, *m*-H), 6.45 (t, 2 H, *p*-H), 2.68 (s, 6 H, CH_3imine), 2.12 (s, 12 H, CH_3) ppm. bmip: ^1H

NMR ($[\text{D}_6]\text{acetone}$): $\delta = 9.53$ (s, 2 H, pz-H), 6.92 (s, 4 H, *m*-H), 2.26 (s, 6 H, CH_3imine), 2.19 (s, 6 H, *p*- CH_3), 2.00 (s, 12 H, *o*- CH_3) ppm. Other reagents were commercially available and used without further purification. All preparations and physical measurements were carried out in dried solvents under argon, using Schlenk techniques.

General Procedure for the Negishi Cross-Coupling Reactions: A solution of aryl iodide (0.5 mmol) in THF (1 mL) was added to the alkylzinc bromide reagent (0.5 mmol) in THF (1 mL) at ambient temperature. To this mixture was added the nickel catalyst (2.5 mol-%) and the hexamethyl benzene (0.5 mmol) internal standard. The resulting mixture was stirred at room temperature and aliquots were checked periodically by GC-MS until all aryl iodide was consumed.

Synthesis of the Complexes

General Procedure for the Preparation of the Binuclear Complexes $[\mu\text{-}(\text{N}^{\wedge}\text{N})\{\text{Ni}(\text{Mes})\text{Br}\}_2]$ ($\text{N}^{\wedge}\text{N} = \text{bpip, bdip, btip, bxip, bmip}$): In each reaction 0.45 mmol of the $\text{N}^{\wedge}\text{N}$ ligand [141 mg of bpip, 154 mg of btip, 167 mg of bxip (or bdip), or 180 mg of bmip] were suspended in toluene (100 mL) together with $[(\text{PPh}_3)_2\text{Ni}(\text{Mes})\text{Br}]$ (707 mg, 0.90 mmol) and stirred for three days at ambient temperature giving dark green reaction mixtures. The solvent was evaporated to dryness and the residue was washed three times with 10-mL *n*-heptane and pentane. The dark green products had to be recrystallised from $\text{CH}_2\text{Cl}_2/n$ -heptane (1:1) to remove unreacted $[(\text{PPh}_3)_2\text{Ni}(\text{Mes})\text{Br}]$.

Thus, we obtained $[\mu\text{-bpip}\{\text{Ni}(\text{Mes})\text{Br}\}_2]$ (224 mg, 0.27 mmol, 60%) as a dark green powder. $\text{C}_{38}\text{H}_{40}\text{Br}_2\text{N}_4\text{Ni}_2$ (829.99): calcd. C 54.99, H 4.86, N 6.75; found C 54.91, H 4.82, N 6.77. ^1H NMR (CD_2Cl_2): *trans* isomer: $\delta = 9.63$ (s, 2 H, Hpz), 7.7–7.2 (m, 10 H, Ph), 5.67 (s, 4 H, *m*-H), 2.71 (s, 6 H, CH_3imine), 2.25 (s, 12 H, *o*- CH_3), 2.19 (s, 6 H, *p*- CH_3) ppm; *cis* isomer: $\delta = 7.68$ –7.45 (m, 10 H, HPh), 6.91 (s, 2 H, Hpz), 6.78 (s, 4 H, *m*-H), 2.36 (s, 6 H, CH_3imine), 2.25 (s, 12 H, *o*- CH_3), 2.23 (s, 6 H, *p*- CH_3) ppm.

$[\mu\text{-bdip}\{\text{Ni}(\text{Mes})\text{Br}\}_2]$ (284 mg, 0.32 mmol, 72%) was obtained as an emerald green microcrystalline powder. $\text{C}_{42}\text{H}_{48}\text{Br}_2\text{N}_4\text{Ni}_2$ (886.05): calcd. C 56.93, H 5.46, N 6.32; found C 56.88, H 5.42, N 6.27. ^1H NMR: *cis* isomer (CD_2Cl_2): $\delta = 7.35$ (s, 2 H, Hpz), 7.19 (s, 4 H, *m*-HMesNi), 6.90 (s, 2 H, *p*-HXyl), 6.75 (s, 4 H, *m*-HXyl), 2.82 (s, 12 H, *o*- CH_3Xyl), 2.30 (s, 12 H, *o*- CH_3MesNi), 2.28 (s, 6 H, *p*- CH_3MesNi), 1.47 (s, 6 H, CH_3imine) ppm.

$[\mu\text{-btip}\{\text{Ni}(\text{Mes})\text{Br}\}_2]$ (257 mg, 0.30 mmol, 67%) was obtained as an emerald green microcrystalline powder. $\text{C}_{40}\text{H}_{44}\text{Br}_2\text{N}_4\text{Ni}_2$ (858.00): calcd. C 55.99, H 5.17, N 6.53; found C 56.03, H 5.20, N 6.54. ^1H NMR: *cis* isomer (CD_2Cl_2): $\delta = 7.37$ (s, 2 H, Hpz), 7.35–7.25 (m, 6 H, HTol), 6.94 (t, 2 H, *p*-HTol), 6.64 (s, 4 H, *m*-HMesNi), 2.75 (dd, 6 H, *o*- CH_3MesNi), 2.68 (dd, 6 H, *o*- CH_3MesNi), 2.37 (s, 6 H, CH_3Tol), 2.22 (s, 6 H, *p*- CH_3MesNi), 1.51 (s, 6 H, CH_3imine) ppm.

$[\mu\text{-bxip}\{\text{Ni}(\text{Mes})\text{Br}\}_2]$ (370 mg, 0.42 mmol, 93%) was obtained as an emerald green microcrystalline powder. $\text{C}_{42}\text{H}_{48}\text{Br}_2\text{N}_4\text{Ni}_2$ (886.09): calcd. C 56.93, H 5.46, N 6.32; found C 56.85, H 5.43, N 6.29. ^1H NMR: *trans* isomer ($[\text{D}_6]\text{acetone}$): $\delta = 9.19$ (s, 2 H, Hpz); 6.85 (s, 4 H, *m*-HMesNi); 6.55 (s, 4 H, *m*-HMesNi); 2.23 (s, 6 H, *p*- CH_3MesNi); 2.21 (s, 12 H, *o*- CH_3MesNi); 2.17 (s, 6 H, *p*- CH_3MesNi); 1.96 (s, 12 H, *o*- CH_3MesNi); 1.60 (s, 6 H, CH_3imine) ppm; *cis* isomer (CD_2Cl_2): $\delta = 7.27$ (s, 2 H, Hpz); 7.19 (s, 4 H, *m*-HMesNi); 6.79 (s, 2 H, *p*-HXylN); 6.65 (s, 4 H, *m*-HXylN); 2.72 (s, 12 H, *o*- CH_3XylN); 2.26 (s, 12 H, *o*- CH_3MesNi); 2.22 (s, 6 H, *p*- CH_3MesNi); 1.46 (s, 6 H, CH_3imine) ppm.

[(μ -bmip){Ni(Mes)Br}₂] (366 mg, 0.40 mmol, 89%) was obtained as an emerald green microcrystalline powder. C₄₄H₅₂Br₂N₄Ni₂ (914.15): calcd. C 57.81, H 5.73, N 6.13; found C 57.85, H 5.73, N 6.13. ¹H NMR ([D₆]acetone): *trans* isomer: δ = 9.19 (s, 2 H, Hpz); 6.85 (s, 4 H, *m*-HMesN); 6.55 (s, 4 H, *m*-HMesNi); 2.23 (s, 6 H, *p*-CH₃MesNi); 2.21 (s, 12 H, *o*-CH₃MesNi); 2.17 (s, 6 H, *p*-CH₃MesN); 1.96 (s, 12 H, *o*-CH₃MesN); 1.60 (s, 6 H, CH₃imine) ppm; *cis* isomer: δ = 7.30 (s, 2 H, Hpz); 6.93 (s, 4 H, *m*-HMesNi); 6.44 (s, 4 H, *m*-HMesN); 2.90 (s, 6 H, *p*-CH₃MesN); 2.78 (s, 6 H, *p*-CH₃MesNi); 2.73 (s, 12 H, *o*-CH₃MesN); 2.29 (s, 12 H, *o*-CH₃MesNi); 2.28 (s, 6 H, CH₃imine) ppm.

Supporting Information (see footnote on the first page of this article): Figures showing the crystal and molecular structure of bmip, further cyclic voltammograms, absorption spectra, and EPR spectra of the radical complexes [μ -(N[•]^N){Ni(Mes)Br}₂]⁻ were provided together with tables containing complete crystallographic data of bmip, DFT-calculated structural data, complete electrochemical and absorption data of the ligands and calculated HOMO and LUMO energies.

Acknowledgments

Stefan Brandholt and Peter Kliesen, University of Cologne, are acknowledged for contributions in preparative work and DSC measurements. C. H. and A. K. are grateful for financial support by the Deutsche Forschungsgemeinschaft (DFG) (KL 1194/4-1 and KL 1194/5-1). D. A. V. thanks the Office of Basic Energy Sciences of the U. S. Department of Energy (DE-FG02-07ER15885) for support.

- [1] a) B. Cornils, W. A. Herrmann (Eds.), *Applied Homogeneous Catalysis with Organometallic Compounds*, 2nd ed., Wiley-VCH, Weinheim, Germany, **2002**; b) S. D. Ittel, L. K. Johnson, M. Brookhart, *Chem. Rev.* **2000**, *100*, 1169–1203; c) A. Michalak, T. Ziegler, *Organometallics* **2001**, *20*, 1521–1532; d) S. Mecking, *Angew. Chem.* **2001**, *113*, 550; *Angew. Chem. Int. Ed.* **2001**, *40*, 534–540; e) V. C. Gibson, S. K. Spitzmesser, *Chem. Rev.* **2003**, *103*, 283–315; f) D. G. Yakhvarov, D. I. Tazeev, O. G. Sinyashin, G. Giambastiani, C. Bianchini, A. M. Segarra, P. Lönnecke, E. Hey-Hawkins, *Polyhedron* **2006**, *25*, 1607–1612; g) D. Meinhard, P. Reuter, B. Rieger, *Organometallics* **2007**, *26*, 751–754; h) F. Speiser, P. Braunstein, L. Saussine, *Acc. Chem. Res.* **2005**, *38*, 784–793.
- [2] a) M. Delferro, T. J. Marks, *Chem. Rev.* **2011**, *111*, 2450–2485; b) Y.-B. Huang, G.-R. Tang, G.-Y. Jin, G.-X. Jin, *Organometallics* **2008**, *27*, 259–269; c) Q. Chen, J. Yu, J. Huang, *Organometallics* **2007**, *26*, 617–625.
- [3] a) C. Moinet, J.-P. Hurvois, A. Jutand, *Adv. Org. Synth.* **2005**, *1*, 403–453; b) C. Amatore, A. Jutand, J. Périchon, Y. Rollin, *Monatsh. Chem.* **2000**, *131*, 1293–1304.
- [4] a) J.-Y. Nédélec, J. Périchon, M. Troupel, *Top. Curr. Chem.* **1997**, *185*, 141–173; b) M. Durandetti, J. Périchon, *Synthesis* **2004**, 3079–3083; c) F. Raynal, R. Barhdadi, J. Périchon, A. Savall, M. Troupel, *Adv. Synth. Catal.* **2002**, *344*, 45–49.
- [5] a) Y. H. Budnikova, *Russ. Chem. Rev.* **2002**, *71*, 111–139; b) D. G. Yakhvarov, Y. H. Budnikova, O. G. Sinyashin, *Russ. J. Electrochem.* **2003**, *39*, 1261–1269; c) D. G. Yakhvarov, Y. H. Budnikova, O. G. Sinyashin, *Mendeleev Commun.* **2002**, 175–176; d) Y. H. Budnikova, J. Périchon, D. G. Yakhvarov, Y. M. Kargin, O. G. Sinyashin, *J. Organomet. Chem.* **2001**, *630*, 185–192; e) Y. H. Budnikova, Y. M. Kargin, J.-Y. Nédélec, J. Périchon, *J. Organomet. Chem.* **1999**, *575*, 63–66.
- [6] A. Klein, Y. H. Budnikova, O. G. Sinyashin, *J. Organomet. Chem.* **2007**, *692*, 3156–3167.
- [7] a) J.-P. Corbet, G. Mignani, *Chem. Rev.* **2006**, *106*, 2651–2710; b) E. J. Anctil, G. V. Snieckus, in: *Metal-Catalyzed Cross-Coupling Reactions* (Eds.: A. de Meijere, F. Dieterich), 2nd ed., Wiley-VCH, Weinheim, Germany, **2004**, pp. 761–813.
- [8] a) R. Jana, T. P. Pathak, M. S. Sigman, *Chem. Rev.* **2011**, *111*, 1417–1492; b) B. M. Rosen, K. W. Quasdorf, D. A. Wilson, N. Zhang, A.-M. Resmerita, N. K. Garg, V. Percec, *Chem. Rev.* **2011**, *111*, 1346–1416; c) V. B. Phapale, M. Guisan-Ceinos, E. Bunuel, D. J. Cardenas, *Chem. Eur. J.* **2009**, *15*, 12681–12688.
- [9] W. Harnying, A. Kaiser, A. Klein, A. Berkessel, *Chem. Eur. J.* **2011**, *17*, 4765–4773.
- [10] a) T. Yamamoto, *Synlett* **2003**, *4*, 425–450; b) K. Osakada, T. Yamamoto, *Coord. Chem. Rev.* **2000**, *198*, 379–399; c) T. Yamamoto, S. Wakabayashi, K. Osakada, *J. Organomet. Chem.* **1992**, *428*, 223–237.
- [11] a) T. Yamamoto, M. Abla, Y. Murakami, *Bull. Chem. Soc. Jpn.* **2002**, *75*, 1997–2009; b) T. Yamamoto, M. Abla, *J. Organomet. Chem.* **1997**, *535*, 209–211; c) M. Uchino, K. Asagi, A. Yamamoto, S. Ikeda, *J. Organomet. Chem.* **1975**, *84*, 93–103; d) T. Yamamoto, A. Yamamoto, S. Ikeda, *J. Am. Chem. Soc.* **1971**, *93*, 3350–3359.
- [12] a) G. C. Tucci, R. H. Holm, *J. Am. Chem. Soc.* **1995**, *117*, 6489–6496; b) A. Arcas, P. Royo, *Inorg. Chim. Acta* **1978**, *31*, 97–99; c) A. Arcas, P. Royo, *Inorg. Chim. Acta* **1978**, *30*, 205–207.
- [13] R. F. De Souza, L. C. Simon, M. C. Alves, *J. Catal.* **2003**, *214*, 165–168.
- [14] A. Klein, *Z. Anorg. Allg. Chem.* **2001**, *627*, 645–650.
- [15] a) M. P. Feth, A. Klein, H. Bertagnolli, *Eur. J. Inorg. Chem.* **2003**, 839–852; b) M. P. Feth, A. Klein, H. Bertagnolli, S. Zális, *Eur. J. Inorg. Chem.* **2004**, 2784–2796.
- [16] A. Klein, A.-K. Schmieder, N. Hurkes, C. Hamacher, A. O. Schüren, M. P. Feth, H. Bertagnolli, *Eur. J. Inorg. Chem.* **2010**, 934–941.
- [17] A. Klein, A. Kaiser, W. Wielandt, F. Belaj, E. Wendel, H. Bertagnolli, S. Zális, *Inorg. Chim. Acta* **2008**, *47*, 11324–11333.
- [18] A. Klein, A. Kaiser, B. Sarkar, M. Wanner, J. Fiedler, *Eur. J. Inorg. Chem.* **2007**, 965–976.
- [19] a) W. Kaim, B. Sarkar, *Coord. Chem. Rev.* **2007**, *251*, 584–594; b) W. Kaim, T. Scheiring, M. Weber, J. Fiedler, *Z. Anorg. Allg. Chem.* **2004**, *630*, 1883–1893; c) A. Klein, *Rev. Inorg. Chem.* **2001**, *20*, 283–303.
- [20] a) A. Klein, W. Kaim, F. M. Hornung, J. Fiedler, S. Zális, *Inorg. Chim. Acta* **1997**, *264*, 269–278; b) M. Schwach, H.-D. Hausen, W. Kaim, *Chem. Eur. J.* **1996**, *2*, 446–451; c) W. Kaim, S. Kohlmann, *Inorg. Chem.* **1987**, *26*, 68–77; d) W. Kaim, *Inorg. Chem.* **1984**, *23*, 3365–3368.
- [21] a) S. Berger, A. Klein, M. Wanner, W. Kaim, J. Fiedler, *Inorg. Chem.* **2000**, *39*, 2516–2521; b) A. Klein, V. Kasack, R. Reinhardt, T. Sixt, T. Scheiring, S. Zalis, J. Fiedler, W. Kaim, *J. Chem. Soc., Dalton Trans.* **1999**, 575–582; B. Sarkar, W. Kaim, J. Fiedler, C. Duboc, *J. Am. Chem. Soc.* **2004**, *126*, 14706–14707.
- [22] W. Kaim, A. Klein, M. Glöckle, *Acc. Chem. Res.* **2000**, *33*, 755–763.
- [23] W. Kaim, *Coord. Chem. Rev.* **2001**, *219–221*, 463–488.
- [24] W. Kaim, *Coord. Chem. Rev.* **2002**, *230*, 127–139.
- [25] S. Berger, A. Klein, W. Kaim, J. Fiedler, *Inorg. Chem.* **1998**, *37*, 5664–5671.
- [26] T. Stahl, V. Kasack, W. Kaim, *J. Chem. Soc. Perkin Trans. 2* **1995**, 2127–2131.
- [27] a) V. V. Saraev, P. B. Kraikivskii, D. A. Matveev, S. N. Zelinskii, K. Lammertsma, *Inorg. Chim. Acta* **2006**, *359*, 2314–2320; b) G. Bai, P. Wei, D. W. Stephan, *Organometallics* **2005**, *24*, 5901–5908; c) N. A. Eckert, A. Dinescu, T. R. Cundari, P. L. Holland, *Inorg. Chem.* **2005**, *44*, 7702–7704; d) M. J. Nilges, E. K. Barefield, R. L. Belford, P. H. Davis, *J. Am. Chem. Soc.* **1977**, *99*, 755–760.

- [28] a) M. Krejčík, M. Daňek, F. Hartl, *J. Electroanal. Chem.* **1991**, 317, 179–187; b) W. Kaim, J. Fiedler, *Chem. Soc. Rev.* **2009**, 38, 3373–3382.
- [29] a) G. M. Sheldrick, *SHELXS-97*, Program for the Solution of Crystal Structures, University of Göttingen, Germany, **1997**; b) G. M. Sheldrick, *SHELXL-97*, Program for the Refinement of Crystal Structures, University of Göttingen, Germany, **1997**.
- [30] TURBOMOLE v. 6.3, **2011**, a development of the University of Karlsruhe and Forschungszentrum Karlsruhe GmbH, **1989–2007**; TURBOMOLE GmbH, since **2007**; available from <http://www.turbomole.com>.
- [31] R. Ahlrichs, M. Baer, M. Haeser, H. Horn, C. Koelmel, *Chem. Phys. Lett.* **1989**, 162, 165–169.
- [32] P. Deglmann, F. Furche, C. Ahlrichs, *Chem. Phys. Lett.* **2002**, 362, 511–518.
- [33] F. Weigend, *Phys. Chem. Chem. Phys.* **2006**, 8, 1057–1065.

Received: December 23, 2011
Published Online: March 30, 2012